International Journal of GEOMATE, Dec., 2021, Vol.21, Issue 88, pp.1-11
ISSN: 2186-2982 (P), 2186-2990 (O), Japan, DOI: https://doi.org/10.21660/2021.88.j2377
Geotechnique, Construction Materials and Environment

WAVE INTERACTIONS WITH TRIPLE SUBMERGED JARLAN-TYPE PERFORATED BREAKWATERS

*Mohammad Bana[1], *Moussa S. Elbisy [2] and Turki M. Alaboud[3]

Umm Al-Qura University, Civil Engineering Department, College of Engineering, Saudi Arabia

*Corresponding Author, Received: 24 Oct. 2021, Revised: 15 Nov. 2021, Accepted: 01 Dec. 2021

ABSTRACT: This study examines wave interactions with triple submerged Jarlan-type perforated breakwaters consisting of two perforated front walls and a solid rear wall. A mathematical model based on an eigenfunction expansion method and a least-squares technique for Stokes second-order waves has been developed. The numerical results obtained for limiting cases for the single solid and single perforated breakwater, double submerged solid vertical plates, single solid and double perforated breakwater, and double Jarlan-type perforated breakwater are in agree reasonably well with previous studies and experimental results. The wave transmission C_T; reflection C_R, and energy-loss C_L coefficients, and the horizontal wave force exerted on the front C_{Ff} and rear C_{Fr} walls are examined. The results indicate that the location of the middle wall between the front and rear walls has little effect on C_R, C_T, and C_L. With the increasing value of porous effect parameter G, the values of C_R, C_T, and C_{Fr} first decreased, attained their minimum values, and then increased. However, the C_{Ff} decreased monotonously with the increasing G. The C_R is maximum when $B/L = 0.48n+0.07$ while it is minimum when relative chamber width, $B/L = 0.46n+0.26$ where n equals to (0, 1, 2,...). It also shows that the triple sub-merged Jarlan-type perforated breakwater significantly reduced C_R values and enhanced the structure's wave-absorbing ability compared with the double one. The optimum parameters recommended for engineering design were G = 0.1–0.2, relative sub-merged depth d/h = 0.1–0.2, and B/L = 0.3–0.4. For practical engineering, the proposed model can be used to predict the structure's response during the preliminary design stage.

Keywords: Jarlan-Type Structure, Submerged Breakwater, Analytical Solution, Hydrodynamic Performance

1. INTRODUCTION

Breakwaters are mainly used to protect coasts from erosion, protect harbor facilities, and provide a calm basin for ships by reducing wave-induced disturbances. There are different types of breakwaters, full protection, and partial protection breakwater. There are many types of partial protection breakwaters, including pneumatic and hydraulic, submerged, floating, flexible floating, detached, perforated, pile, pipe, and slotted breakwaters. The flow behavior through permeable submerged breakwaters is complicated and requires further study to determine its hydrodynamic characteristics and performance efficiency in response to waves.

Researchers have attempted to solve the problem of wave reflection and scouring at the breakwater toe by using perforated walls. Jarlan [1] proposed a breakwater with a perforated front wall and a solid rear wall. Isaacson et al. [2] investigated wave interaction with double slotted barriers numerically and experimentally. They found that the analytical results agree reasonably with the experimental data. Sahoo et al. [3] studied the reflection coefficient (C_R) of a single perforated wall structure. This study showed the C_R to be principally determined by the front-wall porosity and the ratio of the wave chamber width to the incident wavelength. For double- and triple-row breakwaters, Ji and Suh [4] developed a mathematical model that can calculate various hydrodynamic characteristics. According to the results, their mathematical model accurately reproduced most of the experimental findings.

Koraim [5] investigated one row of a vertical slotted breakwater under normal regular waves theoretically and experimentally and developed a simple theoretical model based on an eigenfunction. He tested the model's validity by comparing its results to other studies' theoretical and experimental results. He found that the transmission coefficient (C_T) decreases with increasing values of a dimensionless wave number and wave steepness and decreasing breakwater porosity.

Liu and Le [6] investigated the hydrodynamic performance of wave-absorbing double curtain-wall breakwater. One wall is perforated to the sea-ward side, and the other is impervious to the shoreward side. Two walls extend from above the seawater to some distance above the seabed of the breakwater. They calculated the C_R, C_T, and wave forces acting on the walls and found the obtained numerical results for limiting cases to agree very well with previous predictions for single and double partially immersed impermeable walls.

Liu et al. [7] used a submerged Jarlan-type breakwater consisting of a perforated front wall and a solid rear wall and examined the wave motion analytically and experimentally. Based on matched eigenfunction expansions to develop an analytical solution. The results showed the optimal values for the front wall porosity, the breakwater's relative submerged depth, and the chamber width were 0.1– 0.2, 0.1– 0.2, and 0.3– 0.4, respectively. There will be no effect on the C_T if the perforated front wall is interchanged with the solid rear wall.

Liu et al. [8] investigated wave interactions with a semi-immersed breakwater consisting of a perforated front wall, a solid rear wall, and a horizontal perforated plate between the two walls using wave scattering based on eigenfunction expansions. Additionally, they experimentally investigated C_R, and C_T of the breakwater. The breakwater proved to be more effective at absorbing waves and reducing wave forces.

Alsaydalani et al. [9] studied the hydrodynamic characteristics of three rows of slotted wall breakwaters with permeable and partially immersed front and middle walls, whereas a solid third wall is impermeable. Based on a mathematical model using the eigenfunction expansion method and the least-squares technique to examine the hydrodynamic breakwater performance. The results of the mathematical model adequately reproduce the majority of the important features, according to comparisons with experimental measurements**.**

Elbisy [10] has investigated waves that interact with multiple semi-immersed Jarlan-type perforated breakwaters. The results indicated that when the relative chamber width, $B/L = 0.46n$, C_R is at its highest, and when $B/L = 0.46n+0.24$, (n=0, 1, 2,), it is at its lowest.

Li et al. [11] investigated water wave interaction with a submerged perforated quarter-circular caisson breakwater using analytical solutions and laboratory experiments. Based on linear potential theory, analytical solutions of the problem are developed for normally and obliquely incident waves, respectively. They found that the analytical results agree reasonably with the experimental data.

By extending Liu et al. [7] model, this study describes the flow behavior and the hydraulic performance of triple submerged Jarlan-type perforated breakwaters consisting of two perforated front walls and a solid rear wall. Therefore, examine and develop a numerical model for regular wave interaction of proposed breakwaters. Moreover, validate and assess the performance characteristics of these breakwaters by comparisons between previous studies' measurements of the transmission, reflection, and energy-loss coefficients. The rest of this paper is organized as follows: the analytical solution is developed in section 2. In section 3 the mathematical model is validated. There are also some numerical examples provided. Finally, the main conclusions of this study are summarized.

2. THEORETICAL INVESTIGATION

In this section, numerical solutions have been presented for wave interaction with triple submerged Jarlan-type perforated breakwaters consisting of two perforated front walls and a solid rear wall. The hydraulic performance of these breakwaters depends mainly on a numerical solution using Eigenfunction expansion and the least-squares technique. Hence, the estimation of the wave transmission, reflection, and energy-loss characteristics of the three rows of perforated walls breakwaters under regular linear wave conditions will be obtained.

2.1 Theoretical Formulation and Assumptions

2.1.1 Mathematical formulation

As shown in Fig. 1 schematic diagram of triple vertical walls, the triple permeable submerged Jarlan-type breakwaters, where the front and center walls are permeable and immersed, and third wall is impervious in a water channel. The water depth is h. The submerged depth of the breakwaters, d, is constant, the wall thickness is δ, and the chamber width, B is the distance between the front and back walls. The perforated breakwaters are encountered to regular waves of height H and wavelength L. An axis coordinate system x and z, both are positively oriented. The horizontal coordinate x from left to right and located on the front wall and the vertical coordinate z is positioned upward from the waterline.

The free surface boundary in the water wave problem travels with the velocity of the water particles. One of the unknown factors is velocity. As a result, before calculation, the position of the free surface boundary is likewise an unknown variable before computation. the fluid field the three walls split into four zones. There is a velocity potential that solves the Laplace equation if the fluid is incompressible, and the flow is irrotational. Derived the following boundary value problem for the velocity potential Φ (x, z, t) in each region for monochromatic incoming waves with angular frequency ω and time t:

$$\Phi(x.z.t) = \mathrm{Re}\{\phi\,(x.z)\,e^{-i\omega t}\} \tag{1}$$

The real part of the argument is denoted by $Re[\,]$, the spatial velocity potential denoted by ϕ, and $i = \sqrt{-1}$. By considering an incompressible fluid and irrotational flow motion, the Laplace equation is satisfied by using the velocity potential. The following boundary value problem for the spatial velocity in each region is obtained:

$$\frac{\partial^2\phi_j}{\partial x^2}+\frac{\partial^2\phi_j}{\partial z^2}=0 \quad \text{For } j=1.2.3.4 \tag{2}$$

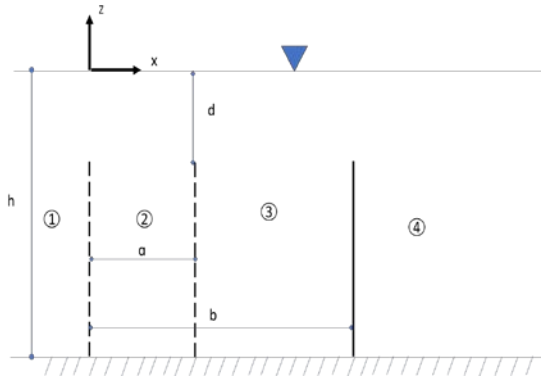

(a)

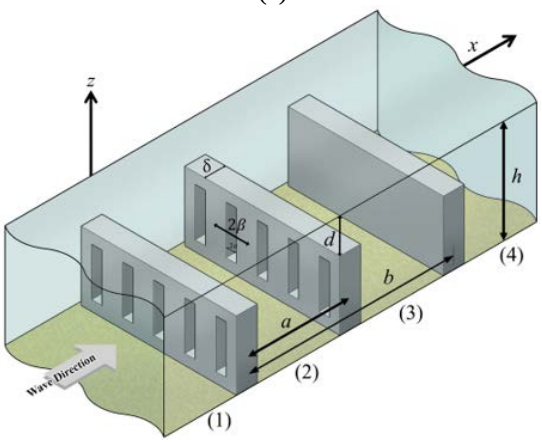

(b)

Fig. 1 Schematic diagram of triple vertical walls, (a) 2D breakwater, and (b) 3D breakwater.

where the variables in the region *j* are represented by the subscript *j*. on the free surface, these potentials must also satisfy appropriate boundary conditions, as the following:

$$\frac{\partial\phi_j}{\partial z}=\frac{\omega^2}{g}\phi_j \quad z=0 \quad j=1.2.3.4 \tag{3}$$

$$\frac{\partial\phi_j}{\partial z}=0 \quad z=-h \quad j=1.2.3.4 \tag{4}$$

$$\lim_{x\to-\infty}\left(\frac{\partial\phi_R}{\partial z}+ik_0\phi_R\right)=0 \tag{5}$$

$$\lim_{x\to\infty}\left(\frac{\partial\phi_4}{\partial z}-ik_0\phi_4\right)=0 \tag{6}$$

By defining the incident wave number by k_0, the gravitational acceleration by g, the velocity potential of the reflected waves by ϕ_R. As well, the reduced velocity potentials ϕ was obtained by using the eigenfunction expansion method that was used by Isaacson et al. [12] and Suh et al. [13]. The velocity potential was expressed by infinite solutions Eq. (2), the solutions satisfied. The boundary conditions of Eq. (3) - (6), as follows:

$$\phi_1=-\frac{igH}{2\omega}\left[e^{-\alpha_0 x}Z_0(z)+R_0e^{\alpha_0 x}Z_0(z)+\sum_{n=1}^{\infty}R_ne^{\alpha_0 x}Z_n(z)\right] \tag{7}$$

$$\phi_2=-\frac{igH}{2\omega}\left[\sum_{n=0}^{\infty}A_ne^{-\alpha_n x}Z_n(z)+\sum_{n=0}^{\infty}\mathrm{C}_ne^{\alpha_n(x-a)}Z_n(z)\right] \tag{8}$$

$$\phi_3=-\frac{igH}{2\omega}\left[\sum_{n=0}^{\infty}B_ne^{-\alpha_n(x-a)}Z_n(z)+\sum_{n=0}^{\infty}\mathrm{D}_ne^{\alpha_n(x-b)}Z_n(z)\right] \tag{9}$$

$$\phi_4=-\frac{igH}{2\omega}\left[T_0e^{-\alpha_0(x-b)}Z_0(z)+\sum_{n=1}^{\infty}\mathrm{T}_ne^{-\alpha_n(x-b)}Z_n(z)\right] \tag{10}$$

By defining the coefficients of the component waves propagating forward and backward by $R_n\,.A_n\,.B_n\,.C_n\,.D_n$ and, T_n (n = 0, 1, 2, …) respectively. The wavenumbers $\alpha=k_n=1,2,...$ are solutions to the first-order dispersion relation $\omega=-gk_n\tan(k_nh)$ (Chakrabarti, [14]; Sarpkaya et al., [15]), In which the propagating evanescent wave and a pair of imaginary roots$\alpha_0=\pm k_0$ for propagating waves have an infinite discrete set of real roots $\pm k_n$ for ($n\geq1$). In Eq. (7)- (10), the negative sign was used so that the propagating waves correspond to the reflected and transmitted waves, respectively. The positive roots of $n\geq1$ was used so that the non-propagating waves fade exponentially with the distance from the wall. The depth-dependent functions *Zn*(*z*) (*n* = 0, 1, 2, …) in Eq. (7)- (10) are as the following:

$$Z_0(z)=\frac{\cosh\mathrm{k}_0(z+h)}{\cosh(k_0h)}\,,Z_n(z)\frac{\cos\mathrm{k}_\mathrm{n}(z+h)}{\cos(k_nh)} \tag{10}$$

Equations (7) -(10) fulfill all the relevant boundaries and automatically fulfill the requirement that is needed to match the horizontal velocities at the breakwater. As a result, the velocity potentials must fulfill the boundary conditions at the interfaces of the breakwater as shown by the following:

$$\frac{\partial\phi_1}{\partial x}=\frac{\partial\phi_2}{\partial x}=i\,k_0\mathrm{G}(\phi_1-\phi_2). \quad x=0. \quad -h\leq z\leq-d \tag{11}$$

$$\frac{\partial\phi_1}{\partial x}=\frac{\partial\phi_2}{\partial x}. \quad x=0. \quad -d\leq z\leq0 \tag{12}$$

$$\phi_1=\phi_2. \quad x=0. \quad -d\leq z\leq0 \tag{13}$$

$$\frac{\partial\phi_2}{\partial x}=\frac{\partial\phi_3}{\partial x}=i\,k_0\mathrm{G}(\phi_2-\phi_3). \tag{14}$$

$x = a. \quad -h \le z \le -d$

$$\frac{\partial \phi_2}{\partial x} = \frac{\partial \phi_3}{\partial x}. \quad x = a. \quad -d \le z \le 0 \qquad (15)$$

$$\phi_2 = \phi_3. \quad x = a. \quad -d \le z \le 0 \qquad (16)$$

$$\frac{\partial \phi_3}{\partial x} = \frac{\partial \phi_4}{\partial x} = 0. \; x = b. \quad -h \le z \le -d \qquad (17)$$

$$\frac{\partial \phi_3}{\partial x} = \frac{\partial \phi_4}{\partial x}. \quad x = b. \quad -d \le z \le 0 \qquad (18)$$

$$\phi_3 = \phi_4. \quad x = b. \quad -d \le z \le 0 \qquad (19)$$

Using from Chwang [16] and Yu [17], *G* is expressed as follows:

$$\mathrm{G} = \frac{\varepsilon}{\delta(f - is)} = |\mathrm{G}|e^{i\theta}. \quad 0 \le \theta \le \pi/2 \qquad (20)$$

"G" is defined as the permeability parameter of a thin perforated well, which is usually complex, and the argument of the complex *G* is $\boldsymbol{\theta}$. When waves pass through a thin of the perforated wall, both a $\boldsymbol{\delta}$ and a wave energy dissipation may happen. The resistance effect of the wall caused the energy dissipation and is relevant to the real part of *G*. The inertial effect of the wall causes the phase shift and is relevant to the imaginary part of *G*. The perforated wall decreases to an impermeable wall when *G* equals zero, and if *G* is shifted toward infinity, the wall is changed to completely transparent. The wall thickness is defined by $\boldsymbol{\delta}$ and the friction coefficient is *f*. The distance between the centers of two neighbor Legs as $\mathbf{2}\boldsymbol{\beta}$ and the opening widens between as $\mathbf{2}\boldsymbol{\alpha}$. The perforated part of the wall porosity is defined as $\boldsymbol{\varepsilon} = \boldsymbol{\alpha}/\boldsymbol{\beta}$ and *s* for the inertia coefficient, as follows:

$$s = 1 + C_m\left(\frac{1-\varepsilon}{\varepsilon}\right) \qquad (21)$$

The added mass Coefficient is *Cm*, it is a constant (*Cm=0*) and *f*= 2.0 as recommended by Isaacson *et al*. [12].

2.1.2. .. Analytic Solution

The expressions for $\phi_j = 1.2.3.4$ fulfill the free Surface, seabed, and convection conditions, in addition to the previously mentioned boundary conditions for $x = xi$, The matching boundary conditions are reduced as follows in Eqs. **(**12**)-(**20**)**:

$$\frac{\partial \phi_1}{\partial x} = \frac{\partial \phi_2}{\partial x}. \quad x = 0 \qquad (22)$$

$$\frac{\partial \phi_1}{\partial x} = i\, k_0 \mathrm{G}(\phi_1 - \phi_2). \quad x = 0. \quad -h \le z \le -d \qquad (23)$$

$$\phi_1 = \phi_2. \quad x = 0. \quad -d \le z \le 0 \qquad (24)$$

$$\frac{\partial \phi_2}{\partial x} = \frac{\partial \phi_3}{\partial x}. \quad x = a \qquad (25)$$

$$\frac{\partial \phi_2}{\partial x} = i\, k_0 \mathrm{G}(\phi_2 - \phi_3). \; x = a. \quad -h \le z \le -d \qquad (26)$$

$$\phi_2 = \phi_3. \quad x = a. \quad -d \le z \le 0 \qquad (27)$$

$$\frac{\partial \phi_3}{\partial x} = \frac{\partial \phi_4}{\partial x}. \quad x = b \qquad (28)$$

$$\frac{\partial \phi_3}{\partial x} = 0. \quad x = b. \quad -h \le z \le -d \qquad (29)$$

$$\phi_3 = \phi_4. \quad x = b. \quad -d \le z \le 0 \qquad (30)$$

Changing the expressions for the velocity potentials in Eqs. (7) and (8) into the boundary condition shown in Eq. (23) gives the following:

$$R_0 = 1 - A_0 + C_0 e^{-\alpha_0 \alpha} \qquad (31)$$

$$R_n = -A_n + C_n e^{-\alpha_0 \alpha}. \quad n = 1.2. \ldots \qquad (32)$$

Changing Eqs. (7) and (8) into the boundary condition shown in Eqs. (24) and (25), with the help of Eqs. (32) and (33), gives the following:

$$2ik_0 G Z_0 + \sum_{n=0}^{\infty}(-2ik_0 G + \alpha_n) A_n Z_n - \sum_{n=0}^{\infty} \alpha C_n Z_n e^{-\alpha_n a} = 0. \quad -h \le z \le -d \qquad (33)$$

$$2Z_0 - 2\sum_{n=0}^{\infty} A_n Z_n = 0. \quad -d \le z \le 0 \qquad (34)$$

Also, changing Eqs. (8) and (9) into the boundary condition shown in equation (26) gives the following:

$$\sum_{n=0}^{\infty} A_n e^{-\alpha_n a} Z_n - \sum_{n=0}^{\infty} B_n Z_n + \sum_{n=0}^{\infty} C_n Z_n + \sum_{n=0}^{\infty} D_n e^{\alpha_n (a-b)} Z_n = 0 \qquad (35)$$

Changing Eqs. (8) and (9) into the boundary condition shown in Eqs. (27) and (28), with the help of Eqs (36), gives the following:

$$\sum_{n=0}^{\infty} -(2ik_0 G + \alpha_0) A_n e^{-\alpha_n a} Z_n - \sum_{n=0}^{\infty} \alpha_n C_n Z_n + \sum_{n=0}^{\infty} 2ik_0 G B_n Z_n = 0 \quad -h \le z \le -d \qquad (36)$$

$$2\sum_{n=0}^{\infty} A_n e^{-\alpha_n a} Z_n - 2\sum_{n=0}^{\infty} B_n Z_n = 0 \quad -d \le z \le 0 \qquad (37)$$

Finally, changing Eqs. (9) and (10) into the boundary condition shown in Eq. (29) gives the following:

$$-B_n e^{-\alpha_n (b-a)} + D_n + T_n = 0. \quad n = 0.1.2. \ldots \qquad (38)$$

If Eqs. (9) and (10) are changed into the boundary condition shown in Eqs. (30) and (31) give the following:

$$\sum_{n=0}^{\infty} -B_n e^{-\alpha_n(b-a)} Z_n + \sum_{n=0}^{\infty} D_n Z_n = 0. \quad -h \le z \le -d \tag{39}$$

$$2\sum_{n=0}^{\infty} D_n Z_n = 0. \qquad -d \le z \le 0 \tag{40}$$

As described by Dalrymple and Martin [18], Eqs. (34), (35), (36), (37), (38), (39), (40), and (41) are known as series relations, and by using the least-squares method, these equations are solved for the values of the coefficients. Along the z-axis, each condition specifies the potential and the function $S(z)$ defined by the boundary condition of the wall as following:

$$S_1^{-h\le z\le -d}(z) = 2ik_0 G Z_0 + \sum_{n=0}^{\infty}(-2ik_0 G + \alpha_n) A_n Z_n - \sum_{n=0}^{\infty} \alpha C_n Z_n e^{-\alpha_n a} \tag{41}$$

$$S_1^{-d\le z\le 0}(z) = 2Z_0 - 2\sum_{n=0}^{\infty} A_n Z_n \tag{42}$$

$$S_2^{-d\le z\le 0}(z) = \sum_{n=0}^{\infty} A_n e^{-\alpha_n a} Z_n - \sum_{n=0}^{\infty} B_n Z_n + \sum_{n=0}^{\infty} C_n Z_n + \sum_{n=0}^{\infty} D_n e^{\alpha_0(a-b)} Z_n \tag{43}$$

$$S_3^{-h\le z\le -d}(z) = \sum_{n=0}^{\infty} -(2ik_0 G + \alpha_0) A_n e^{-\alpha_n a} Z_n - \sum_{n=0}^{\infty} \alpha_n C_n Z_n + \sum_{n=0}^{\infty} 2ik_0 G B_n Z_n \tag{44}$$

$$S_3^{-d\le z\le 0}(z) = 2\sum_{n=0}^{\infty} A_n e^{-\alpha_n a} Z_n - 2\sum_{n=0}^{\infty} B_n Z_n \tag{45}$$

$$S_4^{-h\le z\le -d}(z) = \sum_{n=0}^{\infty} -B_n e^{-\alpha_n(b-a)} Z_n + \sum_{n=0}^{\infty} D_n Z_n \tag{46}$$

$$S_4^{-d\le z\le 0}(z) = 2\sum_{n=0}^{\infty} D_n Z_n \tag{47}$$

2.1.3 Least Squares Technique

As suggested by Dalrymple and Martin [18], the least-squares technique is used to determine the six coefficients, and requires that:

$$\int_{-h}^{0} |S(z)|^2 dz = \text{minimum}, \ h \le z \le 0 \tag{48}$$

For each coefficient and reducing these integral, A_m will give the following:

$$\int_{-h}^{0} S^*(z) \frac{\partial S(z)}{\partial A_m} dz = 0. \ m = 0.1.2. \ldots \tag{49}$$

Defining the complex conjugate of by *S (z)*. And for *z* in Eq. (50) and shortening after *N* terms, gives a set of linear equations as follows:

$$[a_{1mn}]_{N\times N}[A_n^*]_N + [a_{2mn}]_{N\times N}[C_n^*]_N = \tag{50}$$

$$[a_{3mn}]_{N\times N},$$

$$[b_{1mn}]_{N\times N}[A_n^*]_N + [b_{2mn}]_{N\times N}[C_n^*]_N + [b_{3mn}]_{N\times N}[B_n^*]_N + [b_{4mn}]_{N\times N}[D_n^*]_N = 0, \tag{51}$$

$$[c_{1mn}]_{N\times N}[A_n^*]_N + [c_{2mn}]_{N\times N}[C_n^*]_N + [c_{3mn}]_{N\times N}[B_n^*]_N = 0, \tag{52}$$

$$[d_{1mn}]_{N\times N}[B_n^*]_N + [d_{2mn}]_{N\times N}[D_n^*]_N = 0 \tag{53}$$

$$a_{1mn} = (-2ik_0 G + \alpha_m)(2iK_0 G^* + \alpha_n^*) \int_{-h}^{-d} Z_n Z_m dz + 4\int_{-d}^{0} Z_n Z_m dz \tag{54}$$

$$a_{2mn} = (-2ik_0 G + \alpha_m)\left(-\alpha_n^* e^{-\alpha_n^* a}\right) \int_{-h}^{-d} Z_n Z_m dz \tag{55}$$

$$a_{3mn} = (-2ik_0 G + \alpha_m)(2iK_0 G^*) \int_{-h}^{-d} Z_0 Z_m dz + 4\int_{-d}^{0} Z_0 Z_m dz \tag{56}$$

$$b_{1mn} = -e^{-\alpha_n^* a} \int_{-h}^{0} Z_n Z_m dz \tag{57}$$

$$b_{2mn} = -\int_{-h}^{0} Z_n Z_m dz \tag{58}$$

$$b_{3mn} = -\int_{-h}^{0} Z_n Z_m dz \tag{59}$$

$$b_{4mn} = -e^{-\alpha_n^*(a-b)} \int_{-h}^{0} Z_n Z_m dz \tag{60}$$

$$c_{1mn} = \alpha_m(2ik_0 G^* - \alpha_n^*) e^{-\alpha_n^* a} \int_{-h}^{-d} Z_n Z_m dz \tag{61}$$

$$c_{2mn} = \alpha_m \alpha_n^* \int_{-h}^{-d} Z_n Z_m dz \tag{62}$$

$$c_{3mn} = -2ik_0 G^* \alpha_m \int_{-h}^{-d} Z_n Z_m dz \tag{63}$$

$$d_{1mn} = -e^{-\alpha_n^*(a-b)} \int_{-h}^{-d} Z_n Z_m dz \tag{64}$$

$$d_{2mn} = \int_{-h}^{-d} Z_n Z_m dz + 4\int_{-d}^{0} Z_n Z_m dz \tag{65}$$

2.2 Calculation of The Reflection, Transmission, Energy-Loss Coefficients, and Wave Forces:

To obtain the unknown Coefficients A_n^*, B_n^*, C_n^* and D_n^* by using the linear equations (51) -(54) and solving them. Therefore, all the unknown expansion coefficients in the velocity potentials will be determined. In Eq. (7) first part at its right side indicates incident waves propagating by following the positive x-direction, the second part indicates waves from the breakwater, and the third part indicates a series of evanescent modes

degrading in the negative x-direction. As well, in Eq. (10), the first part of the hand indicates transmitted waves propagating in the positive x-direction and the second part indicates a series of evanescent modes degrading in the positive x-direction. Various engineering wave properties can be obtained once the wave potentials are calculated. The real reflection coefficient C_R can be defined as the ratio of the reflected wave height to the incident wave height as the following:

$$C_R = |R_0| \tag{66}$$

The real transmission coefficients C_T is defined as the ratio of the transmitted wave height to the incident wave height, as the following:

$$C_T = |T_0| \tag{67}$$

The energy-loss coefficient C_L is calculated as follows:

$$C_L = \sqrt{1 - C_R^2 - C_T^2} \tag{68}$$

The energy-loss coefficient is equal if $|G|$ is equals to zero or tends toward infinity. The wave force acting on each wall is obtained by integrating the dynamic pressure along with the structure. On the unit width of the front wall F_f, the magnitude of the horizontal wave force is obtained as follows:

$$F_f = i\rho\omega \int_{-d}^{-h} (\phi_1 - \phi_2)\,\big|_{x=0}\, dz = \frac{\rho\omega}{K_0 G} \int_{-d}^{-h} \frac{\partial \phi_1}{\partial x}\,\big|_{x=0}\, dz \tag{69}$$

$$= \frac{\rho g H}{2ik_0 G}\left[(R_0 + 1)\frac{\sinh(k_0 h) - \sinh k_0(d)}{ik_0 \cosh(k_0 h)} + \sum_{n=1}^{\infty} R_n \frac{\sin(k_n h) - \sin k_n(d)}{ik_n \cos(k_n h)}\right] \tag{70}$$

On the unit width of the rear wall F_r, the magnitude of the horizontal wave force is obtained as follows:

$$F_r = i\rho\omega \int_{-d}^{-h} (\phi_3 - \phi_4)\,\big|_{x=0}\, dz \tag{71}$$

$$F_r = \frac{\rho g H}{2}\left[-T_0 \frac{\sinh(k_0 h) - \sinh k_0(d)}{k_0 \cosh(k_0 h)} + \sum_{n=1}^{\infty} (2D_n - T_n)\frac{\sin(k_n h) - \sin k_n(d)}{ik_n \cos(k_n h)}\right] \tag{72}$$

The dimensionless wave forces C_{Ff} and C_{Fr} is defined on the front and rear walls as follows:

$$C_{Ff} = \frac{|F_f|}{\rho g H h} \tag{73}$$

$$C_{Fr} = \frac{|F_r|}{\rho g H h} \tag{74}$$

3. RESULTS AND DISCUSSION

3.1 Validation of the Mathematical Model

The effectiveness of the present model is validated by comparing the calculated results with previous analytical results by Horiguchi [19], Natale [20], Fugazza and Natale [21], Porter's [22], and Liu et al. [7] as well as previous experimental data of Kondo [23].

3.1.1 Comparisons with other Theoretical Models

For a single solid and single perforated breakwater, data from the theoretical results For a double walls (solid and perforated) breakwater, the results of Horiguchi [19] and Natale [20] are considered, in which the water depth, h = 3.0 m, the wave height, H = 1.0 m, the chamber width, B = 4.0 m, d/h = 1.0, and the porosity of the perforated wall, $\varepsilon = 0.3$. As shown in Fig. 2, the results of the present model are close to the theoretical results of Horiguchi [19] and Natale [20].

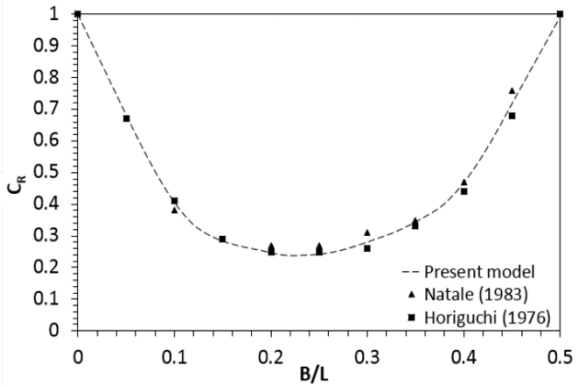

Fig. 2 Comparison of the present model and Horiguchi [19] and Natale [20] results for a single solid and single perforated breakwater.

In addition, for the single solid and single perforated breakwater, data from the theoretical results of Fugazza and Natale [21] are considered, in which H = 4.0 cm, B = 0.5 m, d/h = 1.0, and $\varepsilon = 0.2$. Fig. 3. shows that the present results agree reasonably well with the theoretical results of Fugazza and Natale [21].

When ε of the front walls increases to 1 (the front wall disappears and $G = \infty$) and ε of the second wall decreases to 0 (G = 0), the present breakwater becomes double submerged solid vertical plates. For this case (d/h = 0.1, B/h = 0.5, and G = 0), the present results of C_R and C_T were in identical to the analytical results of Porter [22] , as shown in Fig. 4. Owing to the fluid resonance

between two vertical plates, the multiple local peaks of the C_R could be observed in Fig. 5. This was rather different from the single vertical plate in Fig. 4.

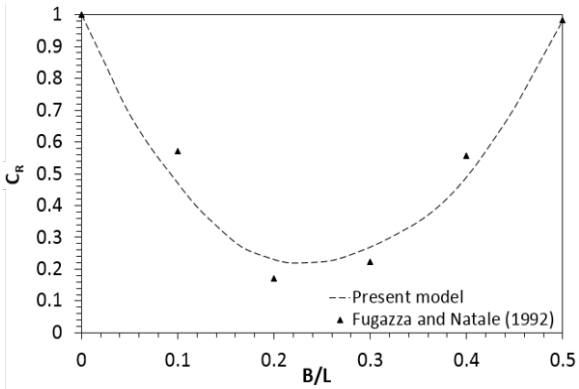

Fig. 3 Comparison of the present model and Fugazza and Natale [21] results for a single solid and single perforated breakwater.

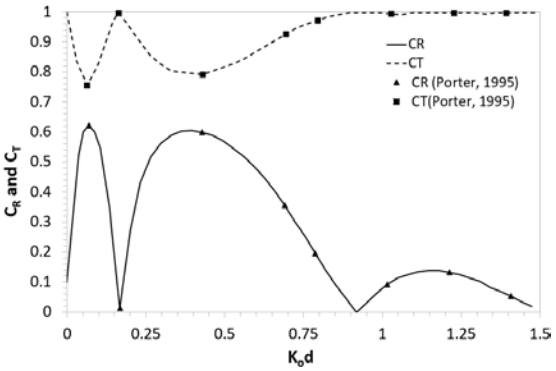

Fig. 4 Comparison of the present model with Porter [22] results for double submerged solid vertical plates at d/h = 0.1, B/h = 0.5, and G = 0.

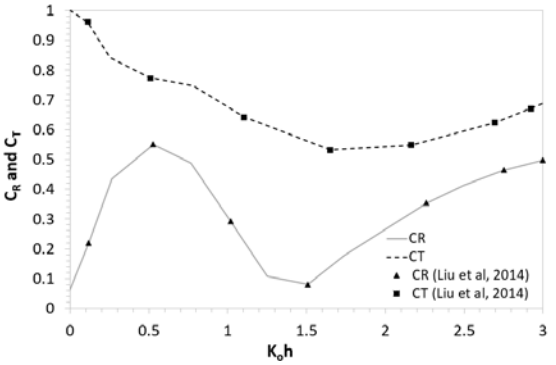

Fig. 5 Comparison of the present model and results of Liu et al. [7] for double Jarlan-type perforated breakwater at d/h = 0.1, B/h = 1.0, and G = 0.5.

Fig. 5 gives a comparison between the present model and the data from the multidomain boundary element method of Liu et al. [7] for submerged Jarlan-type breakwater (perforated front wall and a solid rear wall) at d/h = 0.1, B/h = 1.0, and G = 0.5. It can be seen from Fig. 5 that the present results of C_R and C_T were identical to the analytical results of Liu et al. [7]

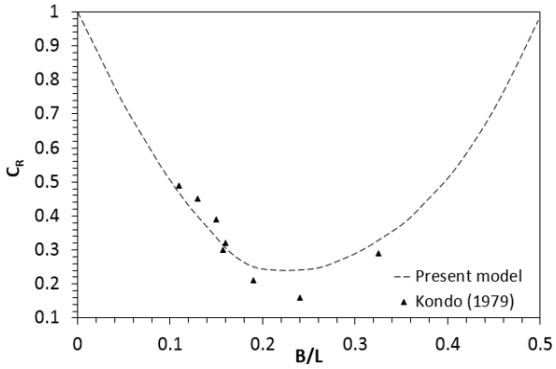

Fig. 6 Comparison between the present model and results of Kondo [23] for the single solid and double perforated breakwater.

3.1.2 Comparisons with Experimental Data

The present model results for the C_R of single and double perforated breakwaters were validated by comparison with the experimental results of Kondo [23]. The porosity of the perforated wall, ε , was 0.2. As shown in Fig. 6, the present results agree well with the experimental results of Kondo [23].

3.2 Numerical Examples

3.2.1 Effect of Relative Submerged Depth

The relationship between the C_R, C_T, *and* C_L of triple submerged Jarlan-type perforated breakwaters and K_oh for different values of d/h (d/h = 0.1, 0.2, and 0.5) with B/h = 2.0, a = b, G = 0.75, and H/h =0.15 are shown in Figs. 7 to 9. It can be seen from these figures that C_T of the breakwater decreased monotonously with the decreasing d/h. This is natural in physics. It seems that d/h = 0.1–0.2 should be an advisable choice for obtaining a smaller C_T. This agrees with the results of Liu et al. [7]. However, the variation in C_R and C_L with increasing d/h is related to K_oh, as shown in Fig. 10.

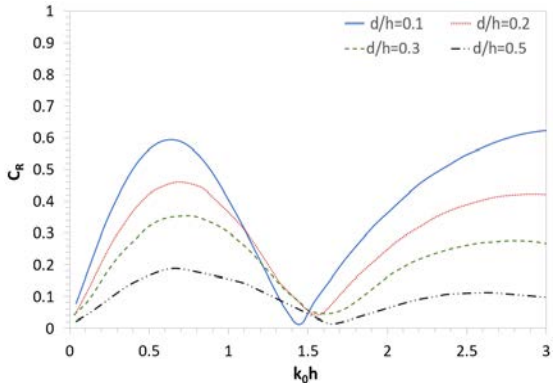

Fig. 4 Effects of the relative submerged depth, on C_R at B/h = 2.0, a = b, G = 0.75, and H/h =0.15.

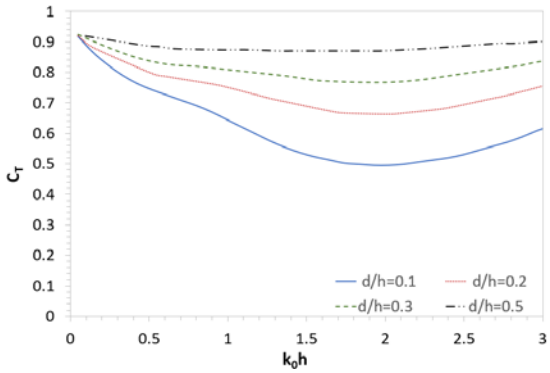

Fig. 5 Effects of the relative submerged depth, on C_T at B/h = 2.0, a = b, G = 0.75, and H/h =0.15.

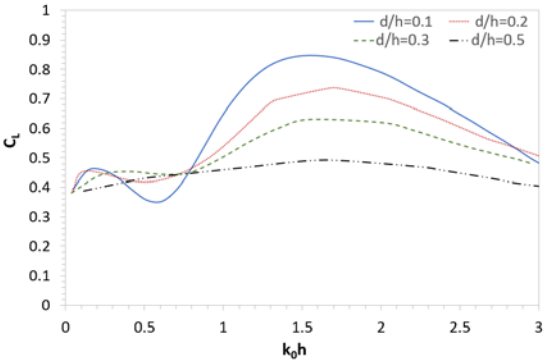

Fig. 6 Effects of the relative submerged depth, on C_L at B/h = 2.0, a = b, G = 0.75, and H/h =0.15.

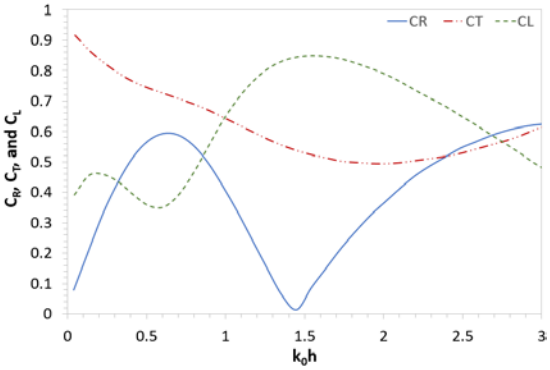

Fig. 10 Variation in the C_R, C_T, and C_L against k_oh with B/h = 2.0, a= b, G = 0.75, H/h =0.15 and d/h = 0.1.

3.2.2 Effect of Relative Chamber Width

Fig. 11 gives the effect of the relative chamber width, B/L, on C_R, C_T, and C_L. It is evident from Fig. 11 that all the hydrodynamic quantities varied periodically with the increasing relative chamber width. Both C_R and C_T oscillate with changing B/L with the same trend. The mentioned effect is due to the dissipation of the wave's energy by the perforated front wall and the C_L oscillation with changing B/L. The variation of the C_R versus the relative chamber width was most remarkable. The maximum value of C_R is when B/L = 0.48n+0.07 *and* its minimum value occurs when B/L = 0.46n+0.26 where n equals to 0, 1, 2... Figure 11 also represents the change in C_L against B/L with opposite maximum and minimum values compared with C_R and C_T.

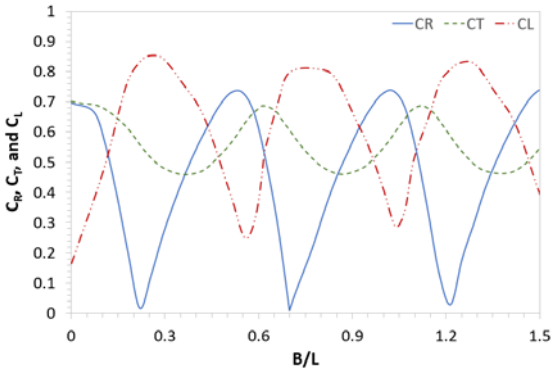

Fig. 7 Variation in the C_R, C_T, and C_L against B/h at k_0h =1.5, a = b, G = 0.75, H/h =0.15, and d/h = 0.1.

3.2.3 Effect of the Front Walls Porous Effect Parameter

Figs. 12 to 14 the effect of the front walls porous effect parameter, G, on C_R, C_T, and C_L. It can be seen from the figures that the C_R, C_T of the present submerged Jarlan-type breakwater may be simultaneously small. This is significant in practice as a small C_T brings good shelter for lee-side regions and a small C_R is beneficial to reduce the seabed scour in front of the structure. With the increasing value of G, the values of C_R, *and* C_T first decreased, attained their minimum values, and then increased. Comparing Fig. 12 and Fig. 5 indicate that the C_R increases with the increase of the number of breakwaters. Moreover, increasing the number of breakwaters produces larger energy dissipation and subsequently reduces the C_T.

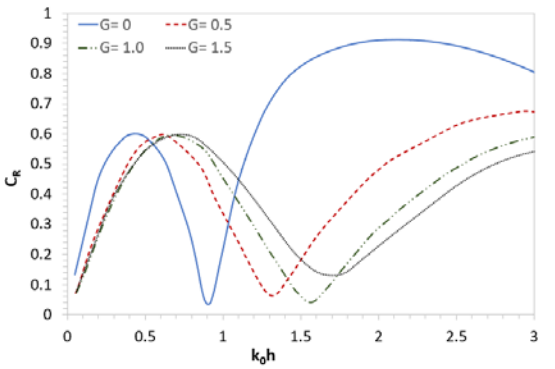

Fig. 8 Variation in the C_R against k_oh with different G at B/h =2.0, a = b, H/h =0.15, and d/h = 0.1.

Figs. 15 and 16 illustrate the effect of the G, on dimensionless wave force on the front wall, C_{Ff}, and dimensionless wave force on the rear wall, C_{Fr} of triple submerged Jarlan-type perforated

breakwaters. the front walls porous effect parameter, G could significantly reduce the wave forces acting on the front and rear walls. This is significant for the safety of the breakwater. A G = 0.5–1.0 is recommended for the submerged Jarlan-type breakwater by considering both good waves absorbing performance and small wave forces. With the increasing value of G, the values of C_{Fr} first decreased, attained their minimum values, and then increased. However, the C_{Ff} decreased monotonously with the increasing G. This was, in fact, the same as those observed in Fig. 15. This agrees with the results of Liu et al. [7].

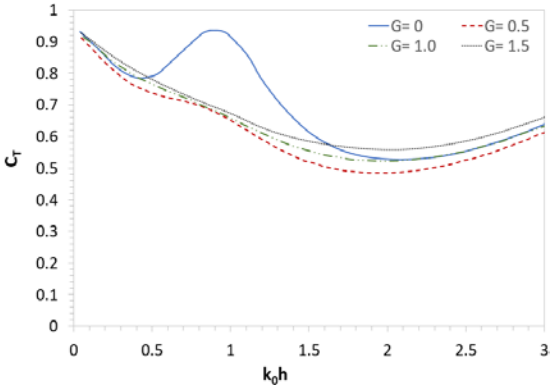

Fig. 9 Variation in the C_T against k_oh with different G at B/h =2.0, a = b, H/h =0.15, and d/h = 0.1.

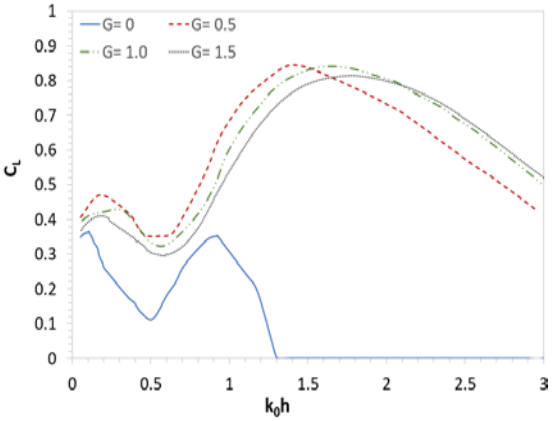

Fig. 10 Variation in the C_L against k_oh with different G at B/h =2.0, a = b, H/h =0.15, and d/h = 0.1.

3.2.4 Effect of the location of the middle wall between the front and rear walls

The location of the middle wall between the front and rear walls is varied three times. Figs. 17, 18, and 19 present the relationship between C_{Ff} and C_{Fr} and B/L for different values of the relative distance between the walls at G = 0.75, H/h =0.15, and d/h = 0.1. From the results, it can be concluded that the location of the middle wall has little effect on C_R, C_T, and C_L. This agrees with the results of Elbisy [10].

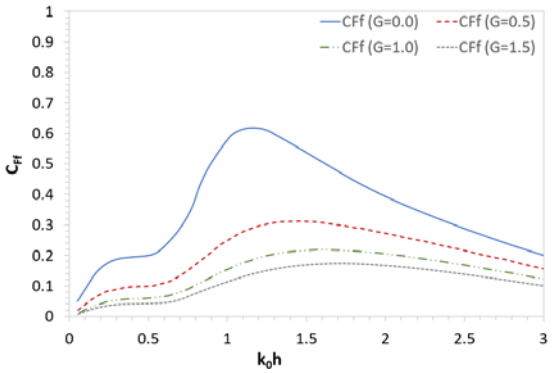

Fig. 15 Variation in the C_{Ff} against k_oh with different G at B/h=2.0, a = b, H/h =0.15, and d/h = 0.1.

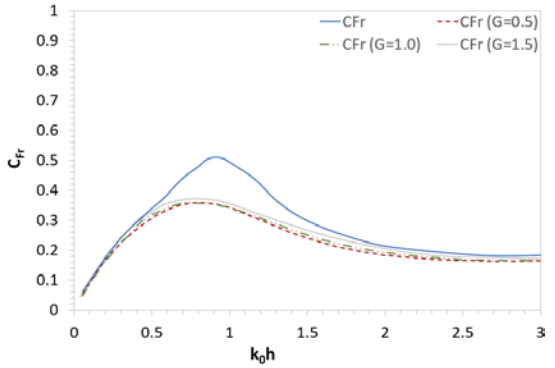

Fig. 16 Variation in the C_{Fr} against k_oh with different G at B/h=2.0, a = b, H/h =0.15, and d/h = 0.1.

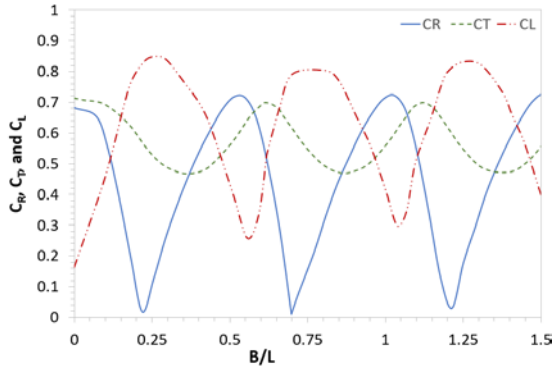

Fig. 17 Variation in the C_R, C_T and C_L against B/L at a= 0.25B, b= 0.75B, G = 0.75, H/h =0.15, and d/h = 0.1.

4. CONCLUSIONS

A mathematical model based on an eigenfunction expansion method and a least-squares technique for linear waves has been developed to study the hydrodynamic performance of triple submerged Jarlan-type perforated breakwaters. The model is validated by comparing the predicted results with the analytical results and the experimental data of previous studies. The comparisons showed that

the results of the presented mathematical model agree reasonably well with the previous analytical results and experimental data. Thus, the model can be used to analyze the performance of triple submerged Jarlan-type perforated breakwaters.

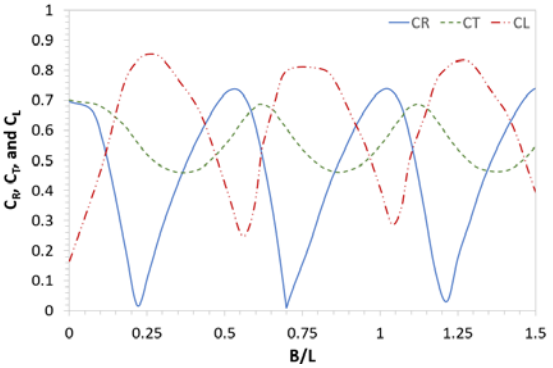

Fig. 18 Variation in the C_R, C_T and C_L against B/L at a= b= 0.5B, G = 0.75, H/h =0.15, and d/h = 0.1.

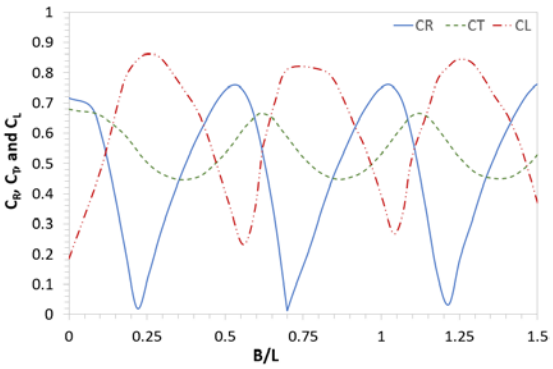

Fig. 19 Variation in the C_R, C_T and C_L against B/L at a= 0.75B, b= 0.25B, G = 0.75, H/h =0.15, and d/h = 0.1.

Numerical examples have shown that compared with triple submerged solid walls, the present breakwater with suitable design had better wave-absorbing performance and lower wave forces. For the triple submerged Jarlan-type perforated breakwater, the optimum parameters (good wave absorbing performance and small wave forces) recommended for engineering design were G = 0.1–0.2, d/h = 0.1–0.2, and B/L = 0.3–0.4.

It is also found that C_R is maximum when B/L = 0.48n+0.07 while it is minimum when B/L = 0.46n+0.26 where n equals to 0, 1, 2.... With the increasing value of G, the values of C_R, C_T, and C_{Fr} first decreased, attained their minimum values, and then increased. However, the C_{Ff} *decreased* monotonously with the increasing G. *Also, it* was found that C_T of the breakwater decreased monotonously with the decreasing d/h. Both C_R and C_T oscillate with changing B/L with the same trend. Also, it was found that the location of the middle wall between the front and rear walls has little effect on C_R, C_T, and C_L.

The triple submerged Jarlan-type perforated breakwater significantly reduced C_R values compared with the double one. Moreover, the triple type was found to be very helpful in enhancing the structure's wave-absorbing ability compared with the double one.

Additional research should be conducted in the future on the triple submerged Jarlan-type perforated breakwater with obliquely incident waves and sea currents.

5. REFERENCES

[1] Jarlan G.E., A Perforated Vertical Breakwater, Dock Harbour Auth., Vol. 41, Issue 486, 1961, pp. 394–398.

[2] Isaacson M., Baldwim J., Premasiro S., and Yang G., Wave interaction with double slotted barriers, Applied Ocean Research, Vol. 21, Issue 2, 1999, pp. 81–91.

[3] Sahoo T., Lee M.M., and Chwang A.T., Trapping and Generation of Waves by Vertical Porous Structures, Journal of Engineering Mechanics, ASCE, Vol. 126, Issue 10, 2000, pp.1074-1082.

[4] Ji C.H., Suh K.D., Wave Interactions with Multiple-Row Curtainwall-Pile Breakwaters, Coastal Engineering, Vol. 57, Issue 5, 2010, pp. 500–512.

[5] Koraim A., Hydrodynamic Characteristics of Slotted Breakwaters under Regular Waves. Journal of Marine Science and Technology, Vol. 16, Issue 3, 2011, pp. 331-342.

[6] Liu Y., and Li. Y., Wave Interaction with a Wave Absorbing Double Curtain-Wall Breakwater, Ocean Engineering, Vol. 38, 2011, pp. 1237–1245.

[7] Liu Y., Xie L., and Zhang Z., The Wave Motion over A Submerged Jarlan-Type Perforated Breakwater, Acta Oceanol. Sin., Vol. 33, Issue 5,2014, pp. 96–102.

[8] Liu Y., Yao Z.L., and Li H.J., Analytical and Experimental Studies on Hydrodynamic Performance of Semi-immersed Jarlan Type Perforated Breakwaters, China Ocean Eng., Vol.29, Issue 6, 2015, pp. 793–806.

[9] Alsaydalani M., Saif M., and Helal M., Hydrodynamic Characteristics of Three Rows of Vertical Slotted Wall Break-waters" J. Marine Sci. Appl., Vol. 16, 2017, pp. 261-275.

[10] Elbisy M., Wave Interactions with Multiple Semi-Immersed Jarlan-Type Perforated Breakwaters, China Ocean Eng., Vol. 31, Issue 3, 2017, pp. 341–349.

[11] Li A., Liu Y., Liu X., and Zhao Y., Analytical and experimental studies on water wave interaction with a submerged perforated quarter-

circular caisson breakwater. Applied Ocean Research, Vol. 101, 2020.

[12] Isaacson M., Premasiro S., and Yang G., Wave Interaction with Vertical Slotted Barrier, Journal Waterway, Port, Coastal and Ocean Eng., Vol. 124, Issue 3, 1998, pp. 118-126.

[13] Suh K.D., Shin S., and Cox D.T., Hydrodynamic Characteristics of Pile-Supported Vertical Wall Breakwaters, J. of Waterways, Port, Coastal and Ocean Engineering, Vol. 132, Issue 2, 2006, pp. 83-96.

[14] Chakrabarti S.K., Hydrodynamics of offshore structures, Computational Mechanics Publications, Southampton, 1987, pp. 57.

[15] Sarpkaya T., Isaacson M., and Wehausen J.V., Mechanics of Wave Forces on Offshore Structures, Journal of Applied Mechanics, Vol. 49, Issue 2,1982, pp. 466-467.

[16] Chwang A.T., A Porous-Wavemaker Theory, Journal of Fluid Mechanics, Vol. 132, 1983, pp. 395-406.

[17] Yu X., Diffraction of Water Waves by Porous Breakwater". J. of Waterway, Port, Coastal and Ocean Engineering, Vol. 121, Issue 6, 1995, pp. 275-282.

[18] Dalrymple R.A., Martin P.A., Wave Diffraction Through Offshore Breakwaters, Journal of Waterway, Port, Coastal and Ocean Engineering, Vol. 116, Issue 6, 1990, pp. 727-741.

[19] Horiguchi T., Wave Dissipation and Forces on a Perforated Caisson Breakwater. Memoirs of Faculty of Tech., 26, Tokyo Metropolitan Univ., Tokyo, Japan, 1976.

[20] Natale L., Reduction of Clapotis in Front of Perforated Breakwaters, Giornale del Genio Civile, 1983, pp. 246-256 (in Italian).

[21] Fugazza M., and Natale L., Hydraulic design of perforated breakwaters". J. Water". J. of Waterway, Port, Coastal, and Ocean Eng., Vol. 118, Issue 1, 1992, pp. 1–14.

[22] Porter R., and Evans D.V., Complementary Approximations to Wave Scattering by Vertical Barriers, Journal of Fluid Mechanics, Vol. 294, 1995, pp. 155-180.

[23] Kondo H., Analysis of Breakwater Having Two Porous Walls. Proc. Coastal Structures, ASCE, Reston, Virginia, USA, 1979, pp. 962–977.